

1 Supplementary Material

2 **Differential contribution of excitatory and inhibitory neurons in shaping**  
3 **neurovascular coupling in different epileptic neural states**

4 Hyun-Kyoung Lim<sup>1,2</sup>, Na-yeon You<sup>1,3</sup>, Sungjun Bae<sup>1,3</sup>, Bok-Man Kang<sup>1,3</sup>, Young-Min Shon<sup>4</sup>,  
5 Seong-Gi Kim<sup>1,3</sup>, Minah Suh<sup>\*1,3,5,6</sup>

6

7 <sup>1</sup>Center for Neuroscience Imaging Research, Institute for Basic Science (IBS), Suwon 16419,  
8 South Korea

9 <sup>2</sup>Department of Biological Sciences, Sungkyunkwan University, Suwon 16419, South Korea

10 <sup>3</sup>Department of Biomedical Engineering, Sungkyunkwan University, Suwon 16419, South  
11 Korea

12 <sup>4</sup>Department of Neurology, Samsung Medical Center, Sungkyunkwan University School of  
13 Medicine, Seoul 06351, South Korea

14 <sup>5</sup>Biomedical Institute for Convergence at SKKU (BICS), Sungkyunkwan University, Suwon  
15 16419, South Korea

16 <sup>6</sup>Samsung Advanced Institute for Health Sciences & Technology (SAIHST), Sungkyunkwan  
17 University, Suwon 16419, South Korea

18

19 *Quantification of vessel diameters and GCaMP6f signals derived from two-photon imaging*  
20 *data*

21 We used a 2D Gaussian filter with a 1.73  $\mu\text{m}$  full width at half maximum (FWHM) to enhance  
22 the signal-to-noise ratio (SNR) of the vessel imaging data. The filtered data were then  
23 processed to correct the movement artifacts using the “StackReg” plugin with a rigid-body  
24 transformation in Fiji.<sup>1</sup> Following this alignment, we selected three to five points on different  
25 branches of pial arterioles and venules within 700  $\mu\text{m}$  from the seizure focus (187 arterioles  
26 and 163 venules from 53 seizures in 8 mice). The identification of the pial arterioles and  
27 venules was based on morphology.<sup>2</sup> Lines perpendicular to the vascular lumens were then made  
28 on the selected points, generating a stack of lines measured over time. To calculate the changes  
29 in vessel diameter, these stacked measurements were then processed using the “Diameter”  
30 plugin in Fiji,<sup>3</sup> which applies a modified algorithm from the full width at half-maximum  
31 (FWHM). Manual measurements from eye inspection evaluated and confirmed the quantified  
32 diameters.

33 To quantify GCaMP6f fluorescence intensity change, we first used Fiji (ImageJ) to apply a  
34 Gaussian filter with a 1.73  $\mu\text{m}$  FWHM kernel to all image stacks in order to improve the signal  
35 to noise ratio. After Gaussian filtering, all image stacks were concatenated for each individual  
36 animal and realigned using the “Image stabilizer” plug-in in Fiji to compensate for potential  
37 in-plane movements. Our field of view (FOV) was 885.76  $\mu\text{m}$  x 885.76  $\mu\text{m}$ , and FOV generally  
38 includes up to 750  $\mu\text{m}$  from the injection focus.

39 The 200  $\mu\text{m}$ -annuli range from the injection focus was excluded to avoid possible damage to  
40 neuronal cells, resulting from the insertion of a glass pipette. The signal intensity was averaged  
41 within the area of 200–700  $\mu\text{m}$  from the 4-AP injection site to quantify changes in excitatory  
42 and inhibitory neuronal calcium activities. The intensity of pixels within 200-700  $\mu\text{m}$  of the

43 seizure focus was averaged in each different epileptic state: pre-injection, preictal and ictal  
44 period, using the same time criteria used for the vessel diameter analysis. To obtain cell  
45 contours of individual neurons (neuron ROIs), we generated a standard deviation (SD) map  
46 using from the 1-min spatiotemporal data following seizure onset. The temporal SD map was  
47 used to identify a cell soma where the calcium changes mainly occurred.

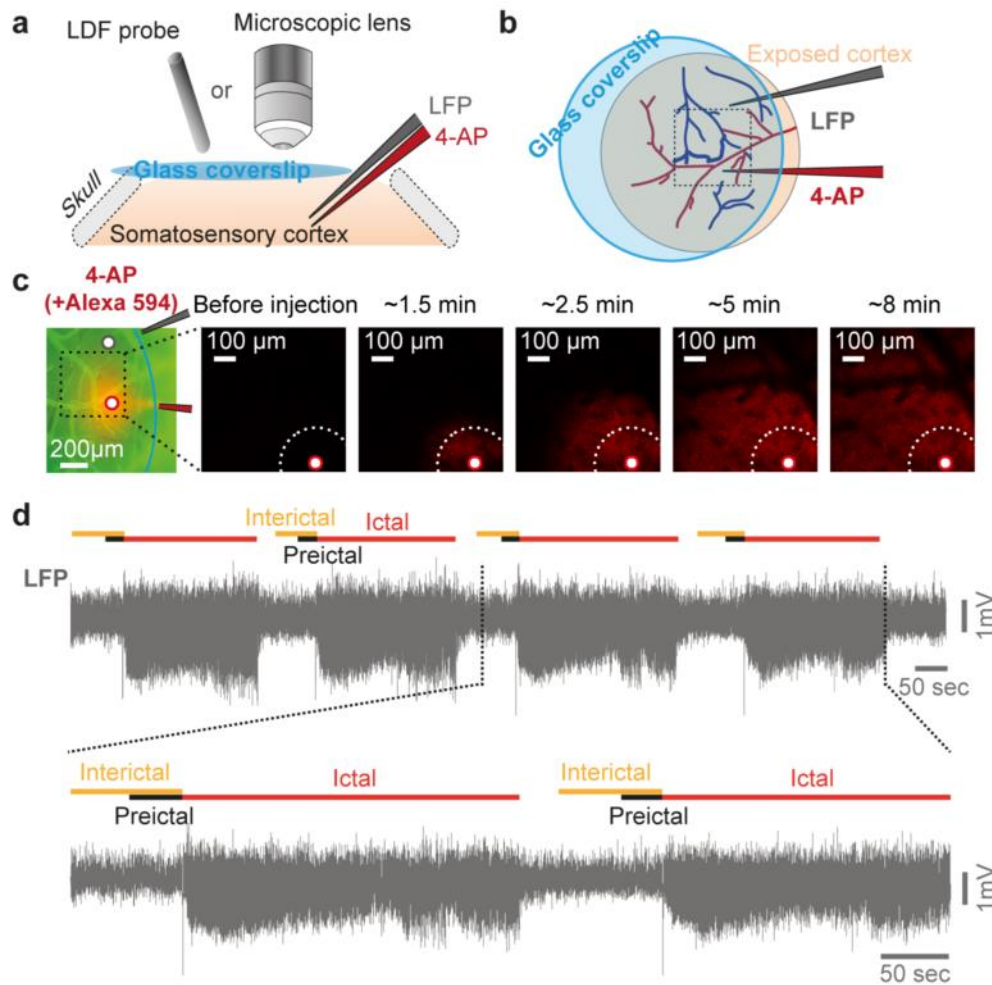
48 To accurately isolate the cell soma regions (neuron ROIs) from the background signal, we  
49 created a  $\sim 20$   $\mu\text{m}$  FWHM kernel Gaussian filtered image and subtracted it from the raw SD  
50 map. A local threshold with "Otsu" algorithm was conducted to cluster the cell soma. After this  
51 transformation, the cell soma clusters were segmented as a single cell shape using a  
52 "watershed" algorithm to divide the boundaries of overlapping cells. We also confirmed the  
53 division visually and excluded clusters with diameters less than 5  $\mu\text{m}$  to eliminate false-positive  
54 signals. The fluorescence time course of each cell was measured by averaging all pixels within  
55 each neuron ROI. We also excluded the clusters whose intensity did not increase more than 2  
56 SD over the preictal level. We then calculated the coordinates of the center of mass of the  
57 defined cell cluster. The distance from the center of the 4AP injection to the cell cluster center  
58 of mass was measured and assigned to the cell cluster. Based on the coordinates of the cell  
59 cluster, the calcium transients of the isolated cells were acquired in each seizure trial. To  
60 calculate neuronal synchrony, we calculated correlation coefficients between a pair of two  
61 neuron ROIs' calcium transients (window: 1s, step: 1s) for all pairs of neuron ROIs identified  
62 in each seizure. In each seizure trial, the correlation values were averaged for the pairs that  
63 showed statistical significance at 95% confidence level.

64

65 *Immunostaining*

66 Anesthetized mice (Zoletil, 30 mg/kg, i.p., Virbac, France) were perfused with saline and 4%  
67 paraformaldehyde (PFA), and their brains were extracted. The brains were fixed in 4% PFA at  
68 4°C for 24 hours and were immersed in 30% sucrose with 0.1% sodium-azide solution for 3  
69 days. The brains were then frozen and coronally sectioned to a thickness of 40- $\mu$ m by cryostat.  
70 The primary antibodies used were mouse anti-green fluorescent protein (GFP, Abcam, USA,  
71 1:200), rabbit anti-neuronal nuclei (NeuN, Abcam, 1:400), rabbit anti-parvalbumin (PV,  
72 Abcam, 1:200), and rabbit anti-somatostatin (SOM, Peninsula, USA, 1:1,000). The secondary  
73 antibodies used were anti-mouse Alexa 488 (Molecular probes, USA, 1:200) and anti-rabbit  
74 Alexa 568 (Molecular probes, 1:350) antibodies. The cell nuclei were stained with 4',6-  
75 diamidino-2-phenylindole (DAPI, Sigma, 1:10,000). The stained brain slices were imaged  
76 using confocal laser microscopy (TCS SP8, Leica).

77



78

79 **Supplementary Figure 1. Experimental set-ups for LDF recording or two-photon imaging**

80 **with concurrent recording of LFP signals and induction of recurrent seizures (a, b)**

81 Schematic drawing of the top and side views of the cranial window, partially covered with a

82 glass coverslip. A glass pipette and an LFP recording probe was intracortically inserted into

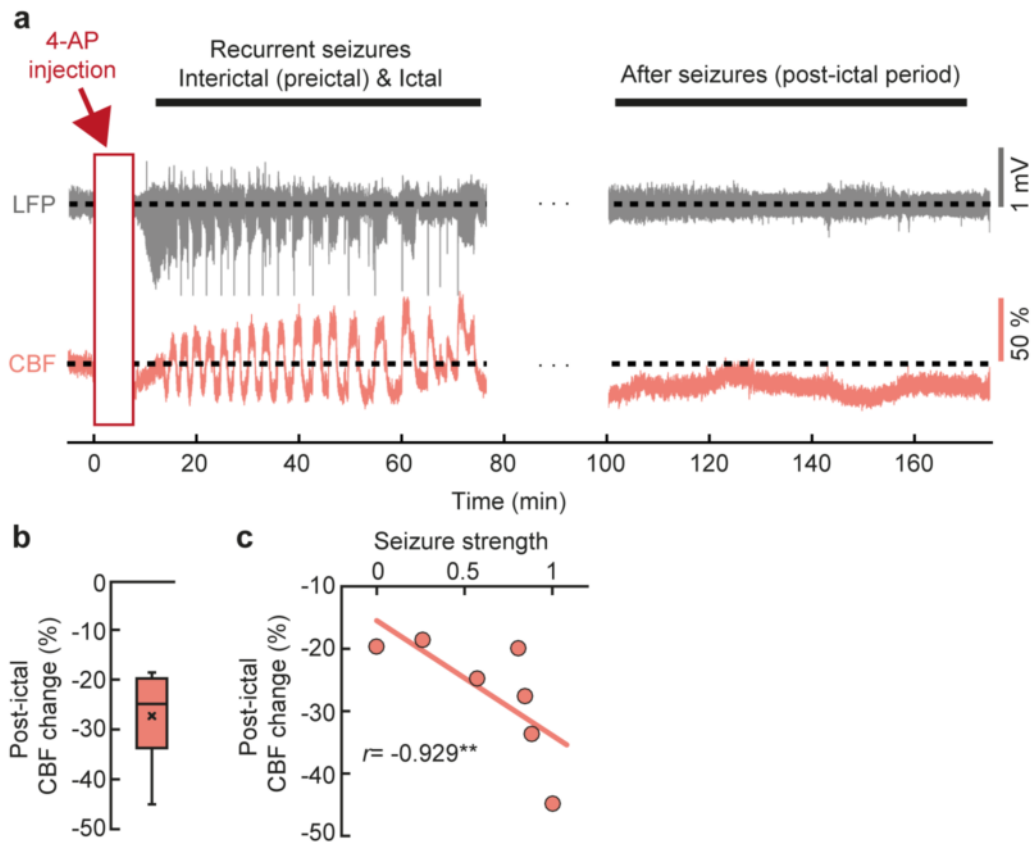
83 layer 2/3 of somatosensory cortex through the partially exposed cranial window. (c) The seizure

84 focus (the tip of the glass pipette) and the temporal spread of the solution are visualized by a

85 mixture of Alexa594 (10  $\mu$ M) with 4-AP (15 mM) to confirm 4-AP injection. (d) An example

86 of LFP signals of consecutive seizures induced by the 4-AP injection, showing different

87 epileptic states: interictal (the period between consecutive seizures), preictal (up to 30 s period  
88 preceding each ictal onset) and ictal events.  
89



90

91 **Supplementary Figure 2. CBF changes after recurrent seizures.** (a) Representative

92 examples showing the dynamics of LFP and CBF before, during and after recurrent seizures

93 induced by 4-AP. (b) Post-ictal CBF changes ( $n=7$ ,  $-26.97 \pm 9.50\%$ , mean  $\pm$  SD). CBF levels

94 during 20-80 mins after last seizure were averaged and normalized according to pre-injection

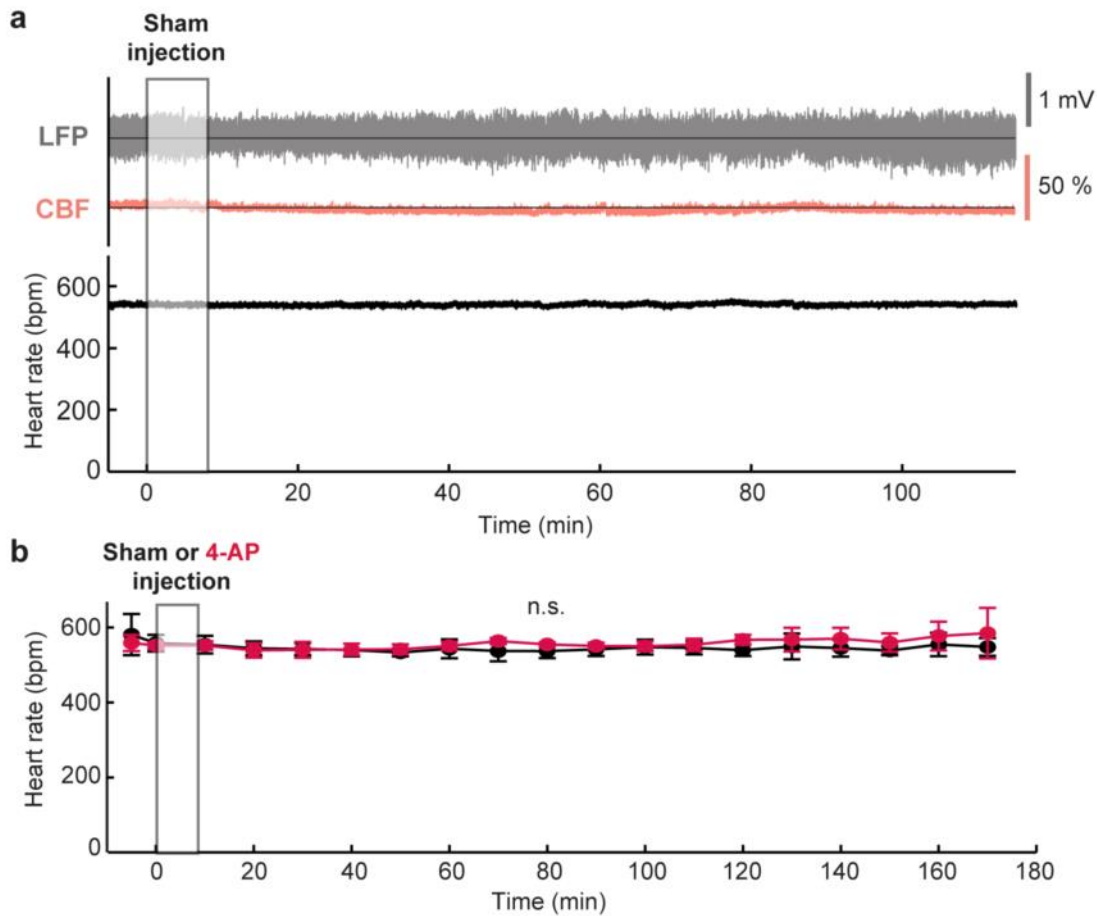
95 CBF levels. (c) Relationship between post-ictal CBF changes and ictal strength of recurrent

96 seizures prior to the post-ictal period (Spearman's  $r=-0.929$ ,  $p=0.007^{**}$ ,  $R^2=0.509$ ). Absolute

97 values of LFP amplitudes ( $>3$  SD above the pre-injection LFP signals) during recurrent seizures

98 were combined to estimate ictal strength.

99



100

101 **Supplementary Figure 3. Time-course traces of LFP signals, CBF changes and heart rate**

102 **in sham control, and heart rate over time in sham or 4-AP injected mice. (a)** Examples of

103 LFP, CBF and heart rate over time in a sham control mouse for ~2 hr, showing no epileptiform

104 activity by using saline injection alone (sham control) without any apparent change in systemic

105 physiological conditions. (b) Averages of the heart rate measured for ~3 hr in mice treated with

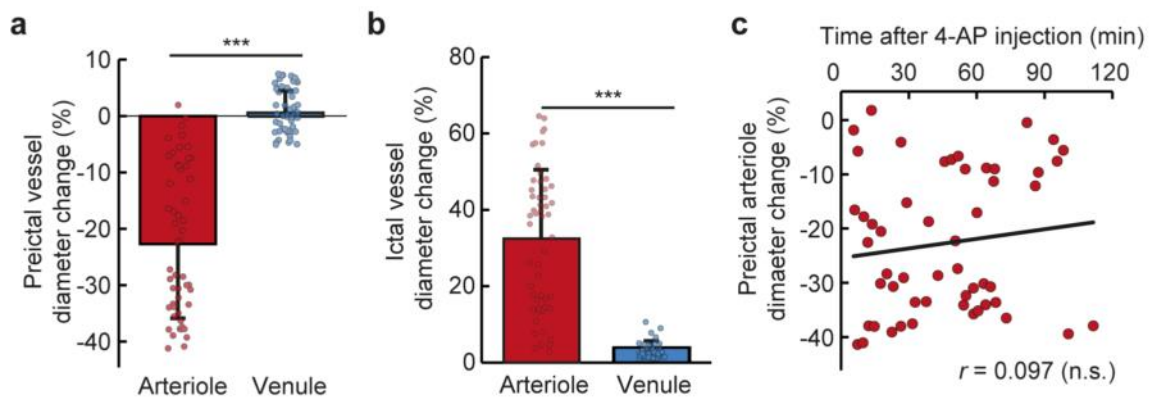
106 sham (n=3, 546.26 ± 20.20 bpm, mean ± SD) and 4-AP injection (n=4, 556.51 ± 10.40 bpm,

107 mean ± SD) (n.s. indicates no statistical significance between the two groups at each time point,

108 tested by Mann-Whitney *U* test) under urethane (1.25 g/kg, i.p.) anesthesia.

109





110

111 **Supplementary Figure 4. Changes in the diameter of preictal and ictal pial vessels**

112 **(arterioles and venules).** (a) Changes in preictal arteriole ( $-22.71 \pm 13.14$  %, mean  $\pm$  SD) and

113 venule ( $0.49 \pm 3.98$  %, mean  $\pm$  SD) diameter (total number of seizures=53, n=8, \*\*\* $p$ <0.001

114 by Mann-Whitney  $U$  test). (b) Maximal diameter changes in arteriole ( $32.32 \pm 18.25$  %, mean

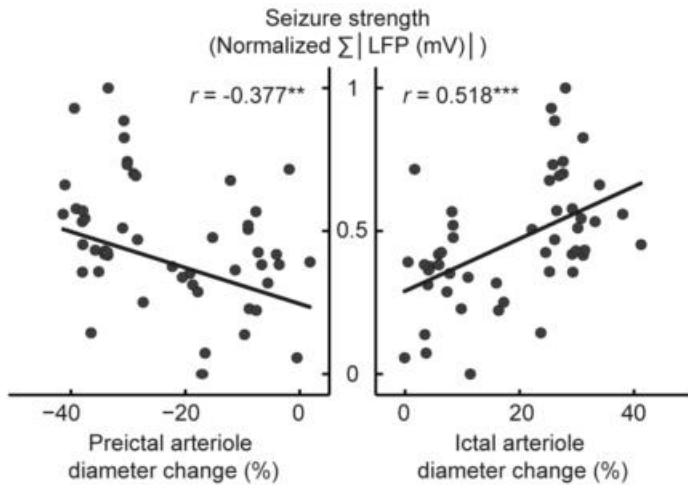
115  $\pm$  SD) and venule ( $3.67 \pm 1.98$  %, mean  $\pm$  SD) during the ictal period (total number of

116 seizures=53, n=8, \*\*\* $p$ <0.001 by Mann-Whitney  $U$  test). (c) Changes in preictal arteriole

117 diameter over time after the 4-AP injection. Preictal arteriole constriction was consistently

118 observed with no significant linear relation with time (total number of seizures=53, n=8,

119 Spearman's  $r=0.097$ ,  $p=0.488$ ; n.s. indicates non- significance).



120

121 **Supplementary Figure 5. Relationship between changes in preictal and ictal arteriole**

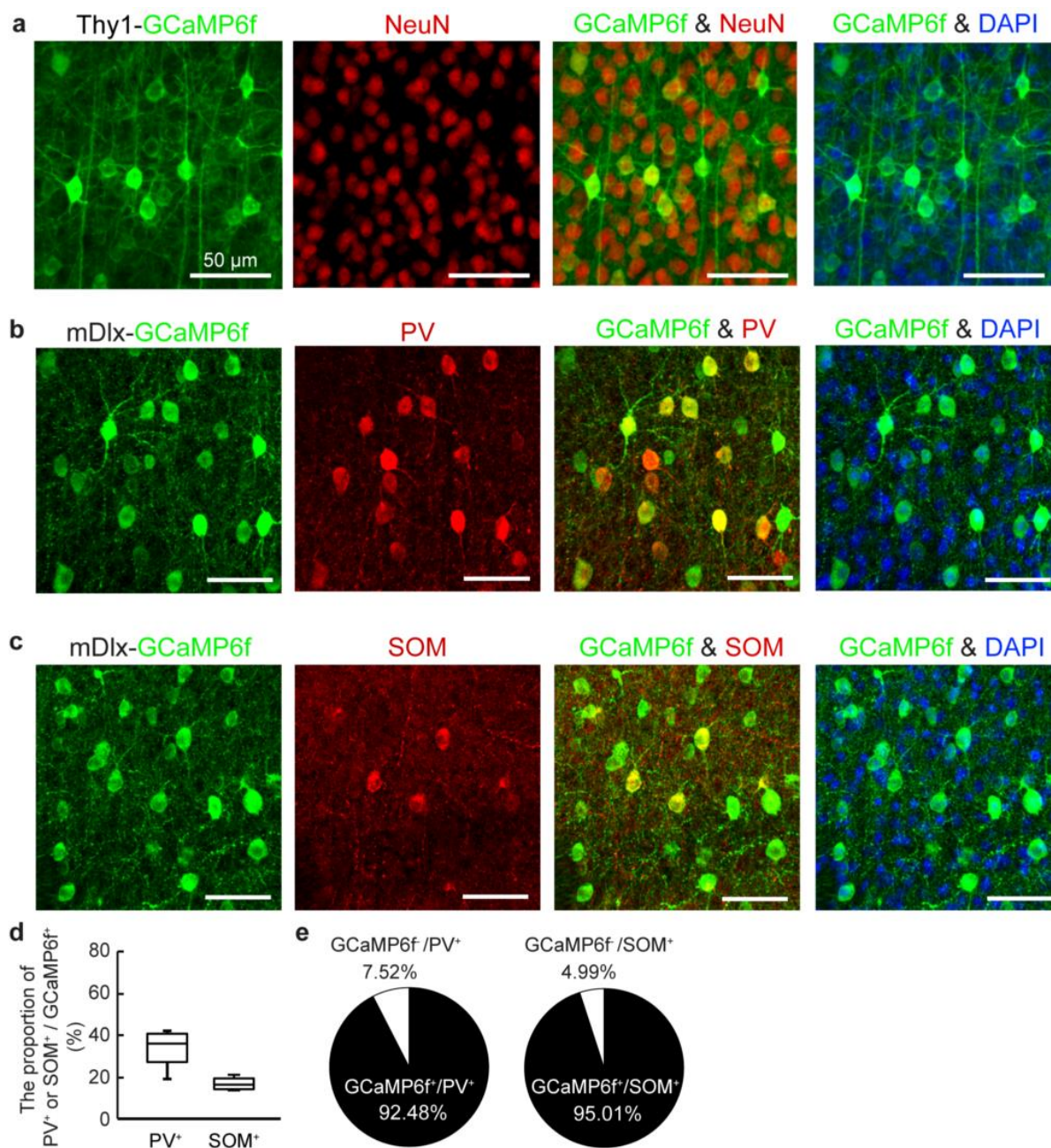
122 **diameter and ictal LFP amplitudes.** The ictal LFP amplitudes were calculated by summing

123 the absolute LFP amplitudes during the period between each seizure onset and offset. The

124 cumulative values were then normalized (total number of seizures=53, n=8, left: Spearman's

125  $r=-0.377$ ,  $**p=0.007$ ,  $R^2=0.145$ ; right: Spearman's  $r=0.518$ ,  $***p<0.001$ ,  $R^2=0.242$ ).

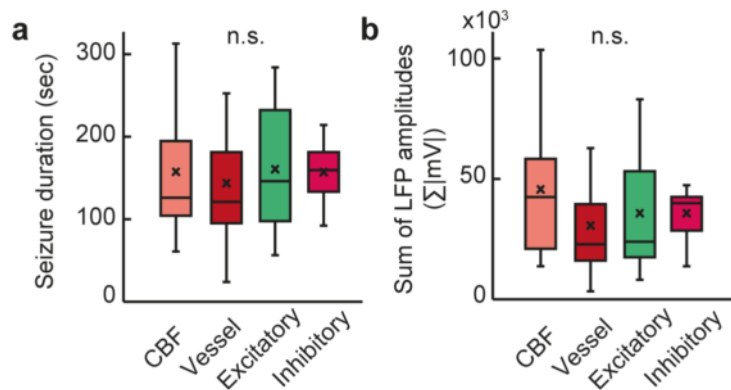
126



127

128 **Supplementary Figure 6. GCaMP6f expression in layer 2/3 of somatosensory cortex in**  
 129 **transgenic mice (Thy1-GCaMP6f-GP5.17DKim/J) and in C57BL/6 mice that receiving**  
 130 **intracortical viral injections (AAV9-mDlx-GCaMP6f-Fishell-2).** (a) Transgenic expression  
 131 of GCaMP6f under Thy1 promoter in mouse somatosensory cortex. GCaMP6f<sup>+</sup> cells were  
 132 overlaid with NeuN<sup>+</sup> cells. Cell nuclei were stained with DAPI. (b-c) Viral expression of

133 GCaMP6f under the mDlx promoter in mouse somatosensory cortex. Representative examples  
134 of colocalization between GCaMP6f<sup>+</sup> cells and PV<sup>+</sup> or SOM<sup>+</sup> cells. (d) Box-whisker diagram  
135 showing the proportions of PV<sup>+</sup> and SOM<sup>+</sup> in GCaMP6f<sup>+</sup> cells (PV<sup>+</sup>:  $33.57 \pm 9.37$  %, SOM<sup>+</sup>:  
136  $17.09 \pm 3.08$  %, n=6, mean  $\pm$  SD) in layer 2/3 of somatosensory cortex. (e) The proportions of  
137 GCaMP6f<sup>+</sup> cells in PV<sup>+</sup> ( $92.48 \pm 9.80$  %, n = 6, mean  $\pm$  SD) and SOM<sup>+</sup> ( $95.01 \pm 4.13$  %, n=6,  
138 mean  $\pm$  SD) cells indicate that the mDlx promoter effectively expressed GCaMP6f in  
139 GABAergic inhibitory neurons.



140

141 **Supplementary Figure 7.** (a) Duration of the seizures measured in the four sets of experiments

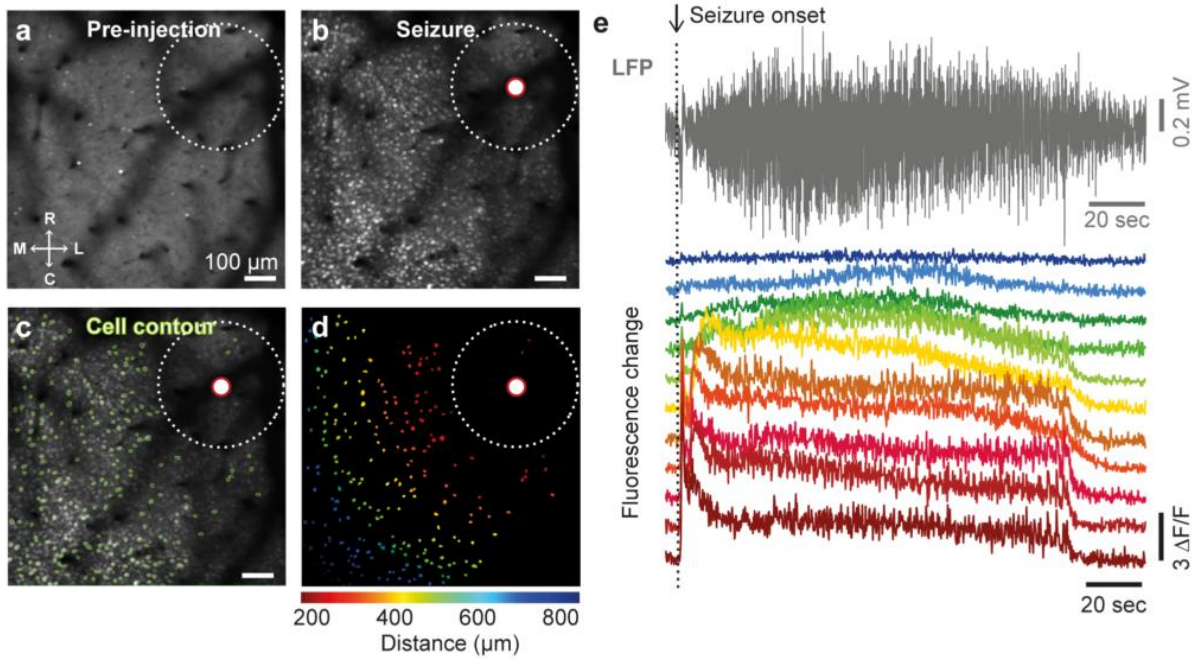
142 (CBF: total number of seizures=42, n=5; Vessel: total number of seizures=53, n=8; Excitatory,

143 total number of seizures=16, n=5; Inhibitory, total number of seizures=19, n=4). (b) Sum of

144 LFP amplitudes between seizure onset and offset in the experiments. Boxes represent 25<sup>th</sup>-75<sup>th</sup>

145 percentiles, and the horizontal lines inside the boxes indicate the medians.

146



147

148 **Supplementary Figure 8. Isolation of neuron ROIs.** (a-b) Representative GCaMP6f  
 149 fluorescence images of neuronal activity before 4-AP injection (pre-injection period) and the  
 150 full ictal event. (c) Contour plot of the registered soma ROIs is overlaid on the ictal image  
 151 shown in (b). (d) Image of the colored neuron ROIs according to their distance from the  
 152 injection focus (red-lined white dot). (e) Example of a seizure event with LFPs and its  
 153 corresponding calcium transient in 11 representative cells within a 200-700 μm range from the  
 154 seizure focus.

155

156 **Supplementary Table 1.**

157 Coefficients of correlation (Pearsons'  $r$ ) between preictal LFP powers at different neural  
 158 frequency bands and the preictal excitatory level shown in Figure 5(g).

	$\delta$	$\theta$	$\alpha$	$\beta$	$\gamma$
$r$	0.368	-0.447	0.368	-0.596	-0.611
$p$ value	0.160	0.083	0.161	0.015*	0.012*
$R^2$	0.136	0.199	0.135	0.355	0.374

159

160 **Supplementary Table 2.**

161 Coefficients of correlation (Pearson's  $r$ ) between the preictal LFP power at different neural  
 162 frequency bands and the preictal inhibitory level shown in Figure 5(g).

	$\delta$	$\theta$	$\alpha$	$\beta$	$\gamma$
$r$	-0.268	0.349	0.535	0.350	0.495
$p$ value	0.268	0.143	0.018*	0.142	0.031*
$R^2$	0.072	0.122	0.286	0.122	0.245

163

164 **Supplementary Movie 1. Examples of spatiotemporal dynamics of preictal and ictal**  
165 **activities of excitatory (left, green) and inhibitory (right, red) neurons.**

166  $\Delta F/F = (F-F_0) / F_0$ , where  $F_0$  represents an average of preictal fluorescence intensity and  $F$   
167 denotes fluorescence intensity over time. The two gray traces below are LFP signals, which  
168 were measured concurrently with excitatory and inhibitory activities, respectively.

169



170 **References**

- 171 1. Thevenaz P, Ruttimann UE and Unser M. A pyramid approach to subpixel registration  
172 based on intensity. *IEEE Trans Image Process* 1998; 7: 27-41. 2008/02/13. DOI:  
173 10.1109/83.650848.
- 174 2. Sakadzic S, Mandeville ET, Gagnon L, et al. Large arteriolar component of oxygen  
175 delivery implies a safe margin of oxygen supply to cerebral tissue. *Nat Commun* 2014; 5: 5734.  
176 2014/12/09. DOI: 10.1038/ncomms6734.
- 177 3. Fischer MJ, Uchida S and Messlinger K. Measurement of meningeal blood vessel  
178 diameter in vivo with a plug-in for ImageJ. *Microvasc Res* 2010; 80: 258-266. 2010/04/22.  
179 DOI: 10.1016/j.mvr.2010.04.004.

180